REVIEW

ADVANCED
ENERGY & SUSTAINABILITY
RESEARCH
Open Access

www.advenergysustres.com

Transition Metal Dichalcogenides Interfacing Photoactive Molecular Components for Managing Energy Conversion Processes

Christina Stangel,* Eleni Nikoli, and Nikos Tagmatarchis*

The remarkable properties of transition metal dichalcogenides (TMDs), represented by molybdenum disulfide (MoS_2), make them promising candidates as active nanomaterials for optoelectronics, electronic, and electrochemical applications. Different exfoliation methods can drastically alter the properties of TMDs, changing the metallic–semiconducting polytype or creating defects, while further chemical surface modification offers additional routes to tune the properties of TMDs by adding new functions. In this timely review, a general outlook on the most representative examples of TMD-based materials interfacing photoactive components, such as porphyrins and phthalocyanines among others, yielding electron donor–acceptor hybrids and nanoensembles for energy conversion schemes, specifically for managing charge transfer events, is presented. The covalent and noncovalent approaches for the coupling of the aforesaid photoactive species with TMDs and their photophysical characterization are highlighted. Moreover, the properties, preparation methods, and characterization techniques of TMDs, mainly for MoS_2, are also briefly discussed. Finally, perspectives and challenges of this emerging area are showcased, aiming to increase scientific attention and enhance not only the performance but also their applicability.

1. Introduction

Transition metal dichalcogenides (TMDs) are materials with the generalized formula MX_2, where M refers to a transition metal from groups 4–7 of the periodic table and X is a chalcogen atom such as S, Se, or Te.[1] The metal cation is bonded to four chalcogenide anions in a honeycomb lattice. This structure forms a three-atom thick layer, where the metals are sandwiched between the chalcogens. Markedly, the chalcogens do not have high

reactivity due to chemical saturation by bonding to the transition metal atoms. These three-atom thick layers are held together with multiple van der Waals forces.[2] However, they can be easily exfoliated by splitting these weak interlayer interactions upon use of a variety of techniques, forming 2D nanosheets with extraordinary physical and chemical properties. In addition, TMDs exist in different lattice structures, which influence the materials' electronic character. Monolayer TMDs have a trigonal prismatic phase (2H phase), that belongs to the D_{3h} symmetry group and corresponds to a trigonal prismatic coordination for the metal atoms, or an octahedral phase (1T phase), that belongs to the D_{3d} symmetry group and corresponds to an octahedral coordination of the metal atoms.[3,4] The 1T phase is metastable and tends to convert to the thermodynamically stable 2H phase at room temperature via intralayer atomic gliding.[5]

The realization of TMD monolayers leads to the confinement of charge carriers in 2D. Thus, due to quantum confinement effects, the transition from indirect bandgap at bulk TMDs, to direct bandgap at few layers and monolayers, occurs,[6] leading to enhanced photoluminescence.[7] Consequently, this is a straightforward approach for tuning the material's photophysical properties. In addition to the aforementioned strategy for obtaining and manipulating the electronic characteristics of TMDs, tuning the materials' properties can be further achieved through doping methods[8] or heterojunctions creation.[9–11] However, due to their atomically thin layers' nature, it becomes impossible to dope TMDs using common techniques that are widely used in semiconductors.[12] In contrast, chemical exfoliation and processing have the advantage of simultaneous modification of the electronic nature of TMDs[13] and in parallel offer the benefit of enhancing dispersibility, allowing surface modification.[14,15] Thus, another way to manipulate the electronic properties of TMDs is by edge or surface functionalization, especially upon incorporation of photoactive molecular species. The latter is a process that has recently emerged for TMDs and considering the advancement already brought in graphene, by the development of numerous functional graphene-based hybrid materials performing in energy conversion schemes under illumination, it certainly deserves further boost.[16–19] Moreover, among various approaches and

C. Stangel, E. Nikoli, N. Tagmatarchis
Theoretical and Physical Chemistry Institute
National Hellenic Research Foundation
48 Vassileos Constantinou Avenue, 11635 Athens, Greece
E-mail: stangel@eie.gr; tagmatar@eie.gr

The ORCID identification number(s) for the author(s) of this article can be found under https://doi.org/10.1002/aesr.202200097.

**ADVANCED
SCIENCE NEWS**

www.advancedsciencenews.com

**ADVANCED
ENERGY & SUSTAINABILITY
RESEARCH**
Open Access

www.advenergysustres.com

worldwide research efforts, combinations of thermally stable mixed–cation perovskites with 2D MoS_2-engineered mesoscopic n–i–p architectures have been used to realize perovskite solar modules. Specifically, and without going deeper in detail, chemically modified MoS_2 by mercaptopropionic acid has been used as an efficient active buffer layer at the perovskite hole transport layer interface and improved the hole injection/collection at the counter electrode.[20] This approach comes to overcome the mismatch of intact MoS_2 valence band (VB) with the perovskite highest occupied molecular orbital (HOMO) level. Beyond filling the defective MoS_2 lattice, functionalization with mercaptopropionic acid effectively shifts the energy band of MoS_2, thereby, allowing to align the VB edge of the latter with the HOMO level of the perovskite and to shift the conduction band (CB) of MoS_2 above the lowest occupied molecular orbital (LUMO) of the perovskite, restricting undesired electron transfer processes. Hence, without surprise, TMDs have attracted significant scientific interest as promising materials in electronic, optical, and catalytic applications, such as in photovoltaics, lithium-ion batteries, photo/electrocatalysis, transistors, sensors, and memory devices.[21–28]

Generally, there are two basic approaches for manufacturing TMD nanosheets, namely, bottom-up and top-down. The bottom-up approach refers to synthetic procedures in which simple units chemically assemble into larger structures. Microwave irradiation, chemical vapor deposition, and wet-chemical procedures, such as hydro/solvothermal, are widely applied in TMD bottom-up synthesis.[29–33] In contrast, top-down realization of TMDs is accomplished via physical methods, such as milling and mechanical or chemical exfoliation as well as molecular intercalation or other thinning methods.[34] Notably, great attention in the top-down preparation of TMDs has been given to liquid-mediated exfoliation,[35] lithium intercalation,[36,37] and electrochemically assisted lithium intercalation.[38] As previously mentioned, upon exfoliation of TMDs, phase transition from the 2H-semiconducting phase to the 1T-metallic one usually occurs. However, every TMD requires a different amount of energy to transit between 2H and 1T phases.[35] Such phase transition has been identified either by treating a chemical vapor deposition (CVD)-grown monolayer with n-butyllithium[39] or by liquid exfoliation with n-butyllithium treatment of bulk TMDs via Li intercalation into the lattice.[40] In contrast, upon liquid exfoliation via a superacid, such as chlorosulfonic acid, intercalation of MoS_2 and WS_2, as representative species of the wider family of TMDs, proceeds with retention of the semiconducting phase of the material.[41] In this case, TMDs act as a weak base due to the presence of the lone electrons of sulfur, which can be protonated by the superacid. Thus, repulsive electrostatic forces are generated, keeping the layers of TMDs apart. Overall and as a general note, the aforementioned techniques for obtaining TMDs have advantages and disadvantages and they are selected according to the application envisioned and/or the specific goal of scientific research. Hence, for example, liquid processing/exfoliation is mainly used for the large-scale production of TMDs, toward functionalization and development of hybrid materials, while CVD grown or micromechanical cleaved allow the investigation of the so-produced TMDs at the nanoscale level due to the ability of controlling the exact number of nanosheet layers.[42]

Functionalization of TMDs is crucial and imperative for tailoring their surface properties and enhancing their dispersion in common solvents, thus allowing better manipulation and expanding the range of applications. A lot of effort has been placed to modify MoS_2, with the methodologies developed being general and applicable to the whole family of TMDs.[14,42] For example, organohalides, maleimides, diazonium salts, 1,2-dithiolanes, and dithiolenes derivatives have been added onto MoS_2.[42–52] A first example of covalent functionalization of TMDs nanosheets, with high functionalization degree, is based on the reaction between the electron-rich metallic 1T phase and an organohalide reactant. Specifically, MoS_2, WS_2, and $MoSe_2$ nanosheets containing a large amount of 1T phase reacted with organohalides and the organic species were covalently attached to the chalcogen atoms of TMDs.[53] Moreover, organothiol derivatives were used to fill S-vacant sites by anchoring to Mo atoms in MoS_2.[54,55] In another approach, when aryl diazonium salts were used for the basal-plane functionalization of 1T-MoS_2, aryl units were incorporated via C—S bonds.[56]

However, the electron-rich 1T phase of TMDS allows for various modification routes, because the reaction is facilitated by electron transfer between reactants and 1T nanosheets (e.g., electrophiles such as diazonium salts and organohalides), the semiconducting phase of TMDs in the absence of defects cannot be easily modified.[14] Nevertheless, functionalization of basal plane or edges of 2H-MoS_2 nanosheets is accomplished upon metal coordination, ligand conjugation with sulfur compounds, and Michael addition reactions. Briefly, the reaction of liquid-exfoliated 2H-MoS_2 with metal acetate salts $M(OAc)_2$ (M=Ni, Cu, Zn) affording functionalized MoS_2–$M(OAc)_2$ materials is one of the first studies in which metal coordination was applied to modify TMDs.[57] Precisely, functionalization occurs via coordination of surface S atoms with the metal center of the metal carboxylate salts. Other examples include interaction of CVD-synthesized 2H-MoS_2 with dibenzothiophene[58] and the reaction of liquid-exfoliated 2H-MoS_2 in the presence of an ionic liquid with thionine.[59] Briefly, in the case of dibenzothiophene, scanning tunneling microscopy analysis revealed that the S-atom of dibenzothiophene coordinates at an S-atom vacancy of MoS_2, forming an S—Mo bond. In contrast, the functionalization of 2H-MoS_2 with thionine is different, and based on X-ray photoelectron spectroscopy (XPS) analysis, it is concluded that the sulfur atom of thionine either coordinates to Mo of MoS_2 (at sulfur defected sites) or forms a disulfide S—S bond with an undercoordinated sulfur atom of the 2D nanomaterial.

The application of organic thiols as S atoms donors is considered as a ligand conjugation approach for 2H-MoS_2 functionalization.[60–67] This strategy describes the formation of a Mo—S bond between S atom of the organic unit and a Mo atom in the MoS_2 structure and was proved by IR spectroscopy, evident by the absence of S—H vibrational modes. Nevertheless, other findings strongly suggest that organic thiols do not form Mo—S bonds, instead organic thiols were oxidized to disulfides that physiosorbed onto the basal plane of MoS_2.[66,67] To avoid the undesired formation and therefore physisorption of disulfides, 1,2-dithiolanes-[50] and dithiolenes[52]-terminated derivatives have been applied as alternatives to fill S vacancies. Recently, it was also reported that 2H-MoS_2 and 2H-WS_2 can be covalently functionalized with maleimide reagents through

ADVANCED
SCIENCE NEWS
www.advancedsciencenews.com

ADVANCED
ENERGY & SUSTAINABILITY
RESEARCH
Open Access
www.advenergysustres.com

Michael addition.[68] This method is based on the soft nucleophilic character of S for interacting with soft electrophiles such as maleimides. The various modes of 2H-MoS$_2$ covalent functionalization are shown in **Figure 1**.

With a variety of methodologies available for modifying TMDs, functional hybrid materials have been designed and prepared. Particularly, photoactive molecular components have been anchored at TMDs using some of the aforementioned general reactions to manage photoinduced charge transfer events[69–73] and prompt charge carrier doping[74–80] as well as charge injection.[81,82] The anchorage of these organic species to TMDs can be via covalent or supramolecular means,[83–87] and the TMDs act as an energy/electron donors or acceptors depending on the relative energy levels of the components constituting the hybrid material. The structural characterization of those modified TMDs relies on complementary techniques. Without going into deeper detail, Raman spectroscopy is a useful tool for identifying the crystal phase structure of TMDs, the number of layers of the nanosheets, and the rate of edge functionalization.[88,89] For example, both 1T-MoS$_2$ and 2H-MoS$_2$ show A_{1g} and E_{2g} vibrational modes at ≈380 and ≈410 cm^{-1}, respectively, but due to

their symmetry differences on the lattice structure, 1T-MoS$_2$ shows additional Raman vibrational bands and the so-called J_1, J_2, and J_3 phonon modes at ≈160, ≈230 cm^{-1}, and ≈330 cm^{-1}, respectively.[36,90,91] In addition, the 2LA(M) mode is vacancy related, and as such it is used to monitor the success and level of functionalization, for example, decrease in the intensity of 2LA(M) upon modification of TMDs.[56,92] In contrast, UV–vis absorption spectroscopy contributes to TMD phase identification. 2H-TMDs nanosheets due to their semiconducting character show characteristic absorption bands due to the direct excitonic transitions and due to the transitions to the density of states between the conduction and the valance band.[93] However, metallic 1T-TMDs do not display absorption bands due to the absence of the energy gap.[94] In addition, photoluminescence is very critical to examine electronic interactions and metallic TMDs do not have emission characteristics due to bandgap absence. Moreover, the number of layers is closely related to the electronic properties of TMDs.[95] The third dimension decreases from the bulk 3D material to the 2D nanosheets, which causes the rich d-orbital interactions, has as consequence the alteration of the electronic band structures and therefore, the
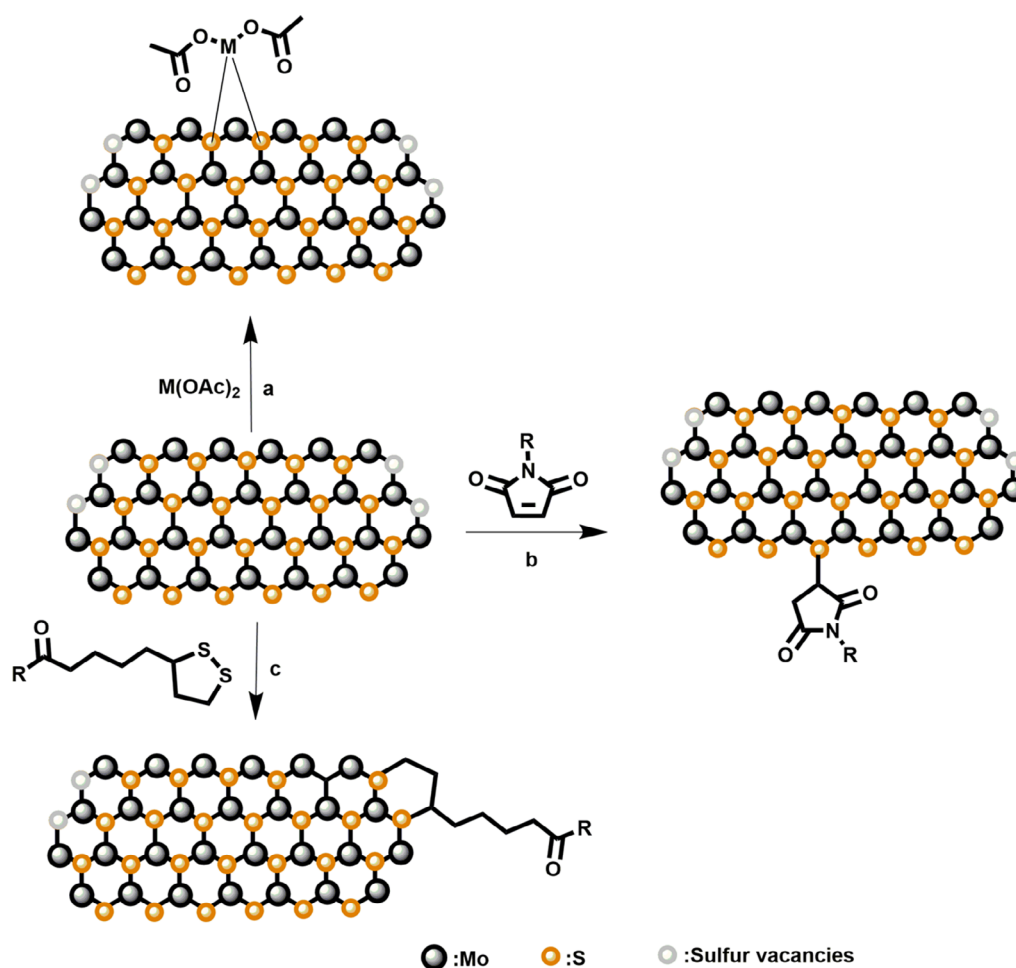
Figure 1. Graphical representation of commonly used covalent functionalization routes of 2H-MoS$_2$: a) coordination of metal acetates, b) maleimides addition, and c) 1,2-dithiolane addition at the edges of MoS$_2$.

**ADVANCED
SCIENCE NEWS**

www.advancedsciencenews.com

**ADVANCED
ENERGY & SUSTAINABILITY
RESEARCH**
Open Access

www.advenergysustres.com

transition of the indirect energy gap of bulk TMDs to direct. This is followed by the dramatic change in the 2D nanosheets' optical properties.[96] For example, bulk MoS$_2$ exhibits a 1.2 eV indirect bandgap, whereas, in the case of a single 2D layer MoS$_2$, the bandgap shifts to direct into 1.8–1.9 eV.[97–102] As it concerns WS$_2$, the bulk form presents an indirect gap and as thins down, it turns into a direct-gap material with an energy gap of 2 eV for monolayer.[103]

Extensive reviews in the recent literature[1,14,104–109] provide significant insight and guidance on the preparation of TMDs and their properties. The current contribution timely complements those and collectively showcases the fast-developing area of modified and functional TMDs, interfacing covalently and supramolecularly photoactive organic components, for tuning their electronic and optical properties and managing the polarity and their charge carriers by performing photoinduced charge transfer processes. Some features of the TMD-based electron donor–acceptor hybrids are discussed in this review, aiming to rationalize structural and electronic effects on the ground and/or excited-state energy/charge transfer dynamics on energy conversion and production to unveil the role of TMDs in the process. To increase the electron transfer rate and slow down charge recombination, simple electron donor–acceptor model systems based on TMDs and photoactive compounds with well-adjusted energies have been developed and studied by using time-resolved ultrafast spectroscopic techniques. In particular, upcoming technological advances should harness the enormous potential of these new materials, with particular emphasis on breakthrough technologies in flexible optoelectronics, photodetectors, and (photo)catalysis. This design strategy offers unique opportunities not only to tune the properties of ultrathin TMDs according to the needs of specific applications, but introduces new functions, aiming to develop new multifunctional materials and devices. Electrical conductivity, together with ambipolar electronic behavior as well as interesting photoluminescence and redox properties, is among the characteristic properties governing and controlling photoinduced activities. Electronic interactions and communication between TMDs and photoactive species occurring under light irradiation, in the form of fundamental studies, have revealed the dual nature of TMDs and are discussed. Particularly the performance of MoS$_2$, acting either as an electron donor or as an acceptor, depending on the relative energy level of the photoactive component at the interface, is highlighted. Despite that porphyrins and phthalocyanines, possessing ideal photo- and electroactive properties, have been employed to modify TMDs, the performance of those hybrid materials in photoinduced energy conversion is far away from the required one when real technological applications are considered. Hence, space for improvement certainly exists, especially by tackling important parameters such as structural, optical, and electronic ones of TMDs interfacing those species. A deeper understanding is required to fine tune the physicochemical and photophysical properties as well as the composition and structural features of the functionalized materials to establish a consistent structure–property relationship. We are confident that this research field will greatly expand by properly addressing those issues and modified TMDs will be implemented in technologically relevant applications. A summary of all those aspects is provided in this review, aiming to enhance the scientific interest of researchers and unlock the opportunities TMD-based materials offer.

2. Photoinduced Charge Transfer Processes in TMDs Covalently Interfacing Photoactive Species

Covalent functionalization with photoactive organic molecules is one of the most efficient ways to fine tune the electronic and physicochemical properties of TMDs in a highly controlled manner. This section provides a summary of findings based on covalent functionalization of TMDs with substituted photosensitizers, while the development of interesting charge transfer phenomena is discussed. Nevertheless, the number of covalently interfaced photoactive species onto TMDs is smaller compared with immobilized ones via noncovalent approaches.
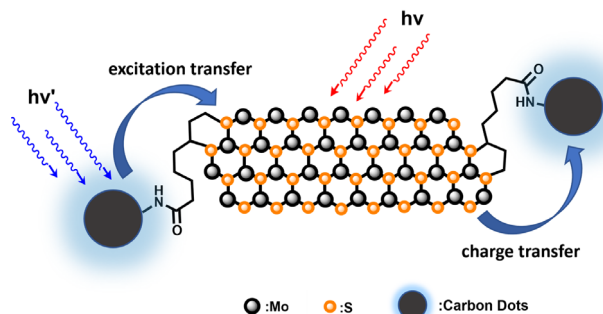
A facile approach for the covalent chemical functionalization of 2H-MoS$_2$ is using 1,2-dithiolane derivatives,[50] possessing high binding affinity for Mo atoms with sulfur-vacant sites. In the particular functionalization methodology, the basal plane remains intact as confirmed by high-resolution transmission electron microscopy and electron energy loss spectroscopy, whereas the addition of the 1,2-dithiolane derivatives occurs at the edges of the nanosheets. Density functional theoretical studies combined with XPS analysis displayed this preferential edge functionalization. When a photoactive pyrene moiety was coupled to a 1,2-dithiolane unit, incorporation of the derivative at the edge sites of the MoS$_2$ yielded the hybrid material MoS$_2$–pyrene.[50] It is interesting to note, not only here but also to all covalent functionalization strategies presented, that the hybrid material generated is filtered through a PTFE membrane, and the solid residue is extensively washed to completely remove any physisorbed species. Spectroscopic IR and Raman assays give proof for the success of functionalization and incorporation of pyrene onto MoS$_2$, while additional evidence for the incorporation of pyrene and estimation of the units grafted came from the thermogravimetric analysis. Notably, steady-state and time-resolved photoluminescence spectroscopy revealed electronic interactions at the excited state, and in particular, electron and/or energy transfer from the pyrene singlet-excited state to 2H-MoS$_2$, implying that MoS$_2$ acts as an electron/energy acceptor. In particular, upon photoexcitation at 340 nm, the emission bands of pyrene were quenched in the hybrid and the fluorescence decay gave rise to a faster component of 280 ps, corresponding to the fluorescence quenching of the emission intensity of the singlet-excited state of pyrene in the MoS$_2$–pyrene hybrid material.

Following the same 1,2-dithiolane functionalization methodology, the covalent incorporation of carbon nanodots (CNDs) onto exfoliated 2H-MoS$_2$ and 2H-WS$_2$ was accomplished.[110] Markedly, CNDs, characterized by an intrinsic emission and broad absorption in the visible region, are promising nanomaterials for energy conversion applications, because they can act as either electron donors or acceptors, owing to their bivalent redox character. The prepared CND-MoS$_2$ and CND-WS$_2$ hybrid materials were fully characterized by complementary IR and Raman spectroscopy, thermogravimetric analysis (TGA), and transmission electron microscopy. Considering the covalent attachment of functionalized CNDs at S-defect sites at the edges of MoS$_2$
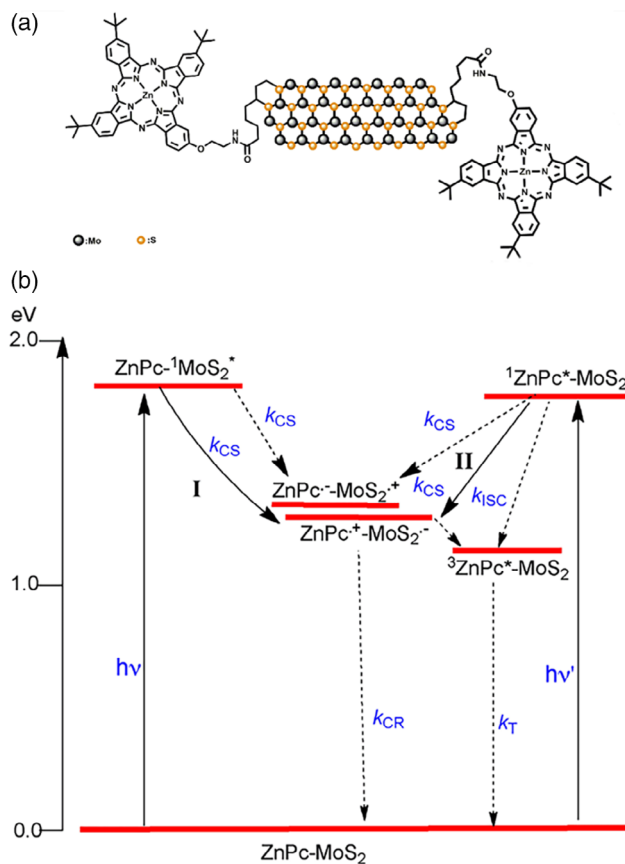
and WS$_2$, the observed mass loss from TGA is relatively small. For CND-MoS$_2$ and CND-WS$_2$, it is 7.5% and 3.0%, respectively, and it is related to the decomposition of modified CNDs present in the two hybrids. Then, the excited-state events were examined by femtosecond pump-probe transient absorption spectroscopy in DMF. Specifically, the hybrids were excited at 370 nm, corresponding mainly to CND excitation, and at 425 nm corresponding mainly to TMD excitation. Markedly, when CND–MoS$_2$ and CND–WS$_2$ were excited at 370 nm, the transient bands corresponding to the excited CNDs revealed rapid deactivation with simultaneous development of strong excitonic peaks of MoS$_2$ and WS$_2$. These findings signify the occurrence of energy transfer from singlet-excited CNDs to MoS$_2$ and WS$_2$ within the hybrids. In both hybrids, this process was complete and efficient within 4–5 ps. Then, upon excitation at 425 nm, charge separation occurred successfully for CND–MoS$_2$ with a time constant of about 250 ps. In addition, from the electrochemical study, a facile oxidation was observed for MoS$_2$ ($E_{pa} = -0.08$ V), indicating that it could act as an electron donor generating a charge-separated state (CSS). A graphical representation of the photoinduced processes that occurred within CNDs–MoS$_2$ is shown in **Figure 2**. In sharp contrast, the transient absorption spectra for CND–WS$_2$ indicated a lack of charge transfer from excited WS$_2$ to CNDs. A possible explanation for that finding could be the harder oxidation of WS$_2$ ($E_{pa} = 0.23$ V).

Next, a substituted zinc phthalocyanine (ZnPc) with a 1,2-dithiolane linker was used to functionalize MoS$_2$ at S-vacant sites,[111] as shown in **Figure 3**a. Phthalocyanines possessing rich electrochemical properties have been covalently attached to electron-accepting fullerenes, carbon nanotubes, and graphene; therefore, CSSs were generated upon illumination. After the spectroscopic, thermal, and microscopy imaging characterization of the ZnPc–MoS$_2$ hybrid, the photoinduced charge transfer events were explored. In particular, fluorescence spectroelectrochemistry revealed direct evidence for the occurrence of charge transfer. Further, the photophysical properties were assessed via femtosecond transient absorption spectroscopy. The finding is that charge separation occurred by direct excitation of either ZnPc or MoS$_2$ and led to the formation of the CSS ZnPc$^{\bullet+}$–MoS$_2^{\bullet-}$. By the absorption and fluorescence spectroscopy as well as redox studies, the energy-level diagram depicting different photochemical events was constructed, as shown in **Figure 4**b. The calculations showed that the formations of ZnPc$^{\bullet+}$–MoS$_2^{\bullet-}$ and ZnPc$^{\bullet-}$–MoS$_2^{\bullet+}$ are both thermodynamically

Figure 3. a) Illustrative structure of ZnPc–MoS$_2$ and b) energy-level diagram showing possible photochemical events occurring within the ZnPc–MoS$_2$ hybrid material. Solid arrows show major processes, while dashed arrows show minor ones. Reproduced with permission.[111] Copyright 2019, John Wiley and Sons.

possible, either from the direct bandgap of MoS$_2$ or ^{1}ZnPc* excitation. However, the formation of ZnPc$^{\bullet+}$–MoS$_2^{\bullet-}$ is more feasible by almost 0.06 eV. The charge separation from excited MoS$_2$ to ZnPc depends on the efficient formation of excitons, biexcitons, and trions, the dissociation of these species into free charge carriers, and the transfer of charges to generate ZnPc$^{\bullet+}$–MoS$_2^{\bullet-}$. Turning to fs-transient absorption (TA) measurements, ZnPc–MoS$_2$ excited at 425 nm, which corresponds mainly to MoS$_2$, at 370 nm, where both MoS$_2$ and ZnPc absorb, and at 675 nm, which mainly excites the ZnPc derivative. The findings revealed charge transfer from ^{1}MoS* to ZnPc and also that the excitation of ZnPc at 675 nm promoted charge transfer, leading to CSSs. In addition, the involvement of excitons generated in MoS$_2$ promotes these charge transfer events.

In addition, other phthalocyanine derivatives bearing sulfenyl and 6-sulfhydryl linkers, abbreviated as ZnPc, were also used to functionalize MoS$_2$ at sulfur vacancies by ligand conjugation,[112] as shown in Figure 4a. MoS$_2$ with sulfur vacancies was prepared by a facile acid-assisted hydrothermal method and then MoS$_2$/ZnPc composites were prepared. In addition, polyvinyl alcohol (PVA) was used for the preparation of films of MoS$_2$/ZnPc/PVA to compare them with the behavior in solution.

Figure 2. Graphical representation of photoinduced processes within CNDs–MoS$_2$.

**ADVANCED
SCIENCE NEWS**

www.advancedsciencenews.com

**ADVANCED
ENERGY & SUSTAINABILITY
RESEARCH**
Open Access

www.advenergysustres.com
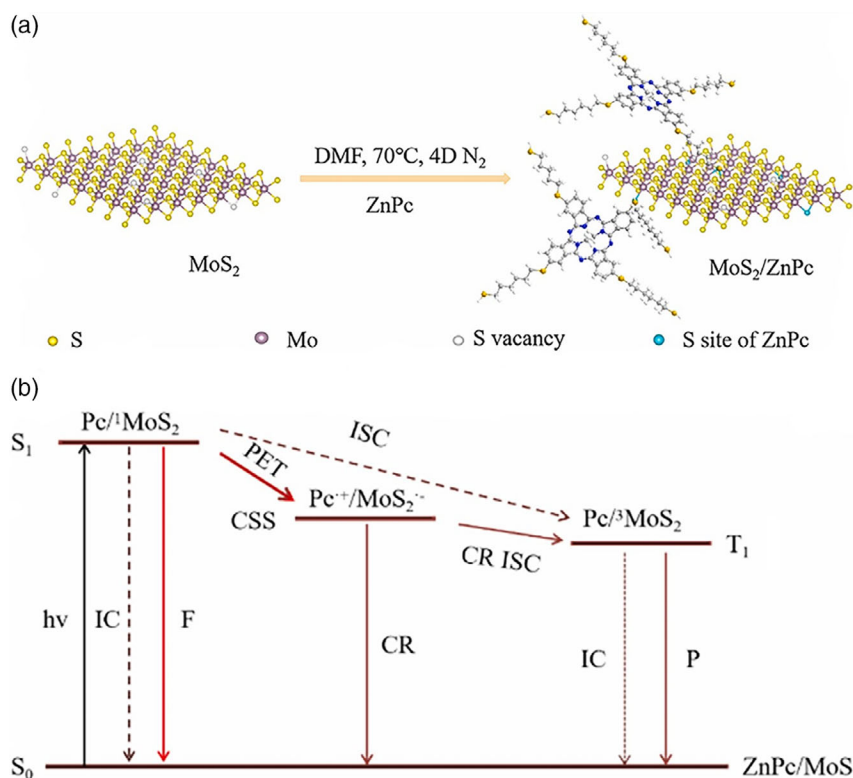
Figure 4. a) Illustrative preparation of ZnPc–MoS$_2$ and b) energy-level model explaining the PET process of ZnPc–MoS$_2$. F: fluorescence; P: phosphorescence; ISC: intersystem crossing; PET: photoinduced electron transfer; CSS: charge-separated state; CR: charge recombination; IC: internal conversion. Reproduced with permission.[112] Copyright 2021, Elsevier.

Photoluminescence measurements indicated electron or energy transfer from ZnPc to MoS$_2$ moiety, when MoS$_2$/ZnPc in DMSO excited at 625 nm, as observed by the quenching of the ZnPc emission at 730 nm. Furthermore, an energy-level model is used to analyze the possible electron transfer process in MoS$_2$/ZnPc composite (Figure 4b). The third-order nonlinear optical (NLO) properties and optical limit (OL) performance, in solution and in films, were studied at 532 nm with 4 ns laser pulses and found that MoS$_2$/ZnPc exhibited much larger NLO properties and OL performance

than those of individual ZnPc and MoS$_2$. It is concluded that the combination of different NLO mechanisms of MoS$_2$ and ZnPc and the electron transfer or energy transfer process between the two components enhanced the performance.[112]
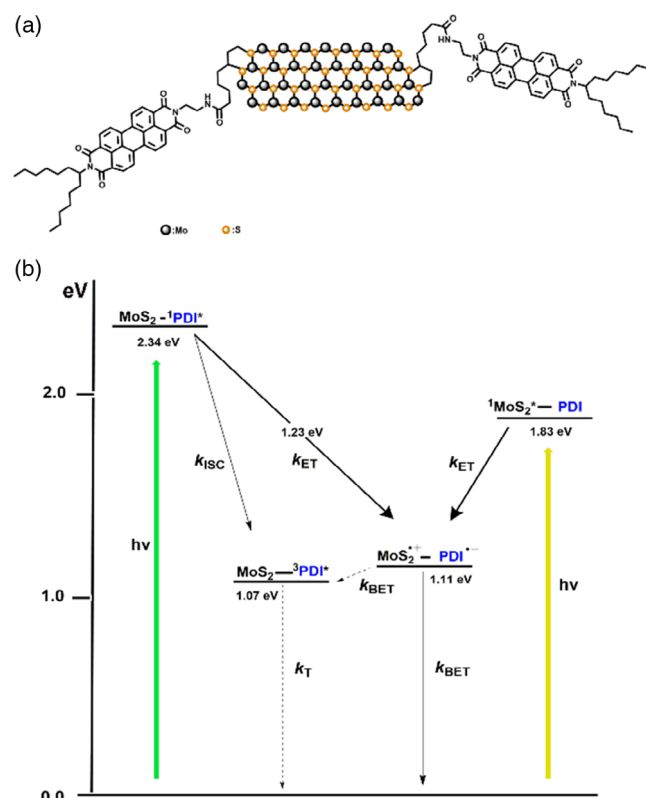
Porphyrins were also conjugated onto TMDs, specifically at the edges of exfoliated 2H-MoS$_2$. **Figure 5**a shows the covalent interface of a porphyrin derivative bearing a 1,2-dithiolane moiety onto MoS$_2$ en route to the preparation of H$_2$P–MoS$_2$.[113] Porphyrins are photochemically stable and absorb efficiently light in the visible region with high molar absorbance coefficients. These photosensitizers are very attractive for participating in charge transfer processes in electron–donor acceptor systems as efficient electron donors. The electronic interactions and exited-state properties were examined via femto- to nanosecond timescales upon photoexcitation. Figure 5b shows the deactivation models for MoS$_2$, H$_2$P–MoS$_2$, and porphyrin upon excitation at 420 nm by means of fs-TA measurements. It was
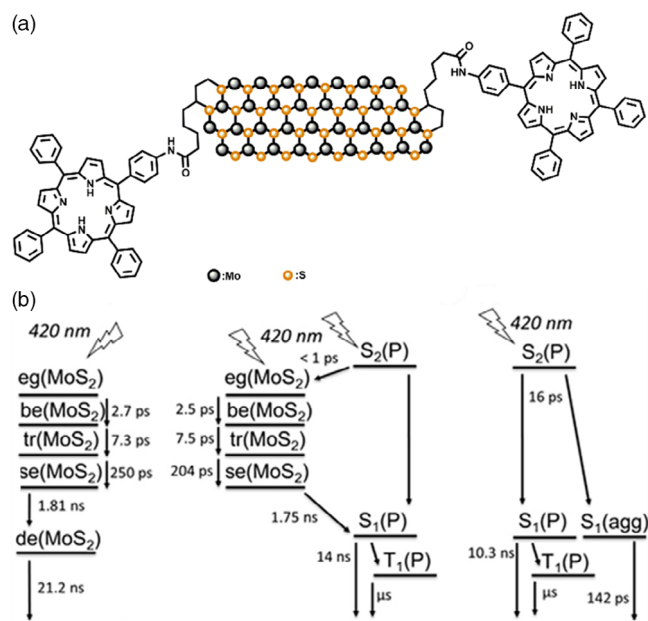
Figure 5. a) Illustrative structure of H$_2$P–MoS$_2$ and b) deactivation models for MoS$_2$ (left), H$_2$P–MoS$_2$ (middle), and H$_2$P (right), upon excitation at 420 nm. Reproduced with permission.[113] Copyright 2019, John Wiley and Sons.

**ADVANCED
SCIENCE NEWS**

www.advancedsciencenews.com

**ADVANCED
ENERGY & SUSTAINABILITY
RESEARCH**
Open Access

www.advenergysustres.com

found that a complex "ping–pong" energy transfer mechanism occurs and in particular a nonquantitative ultrafast energy transfer from the porphyrin to MoS_2 and then back to the porphyrin. In more detail, the energy transfer is <1 ps from porphyrin's S_2, which is populated upon excitation at 420 nm, to MoS_2 (Figure 5b, middle). Then, the formation of single excitons was identified and the times for the interconversions were 2.5, 7.5, and 204 ps. Afterward, the single exciton of MoS_2 is subjected to a second energy transfer to the S_1 state of H_2P and this takes 1.75 ns (Figure 5b, middle).

In all of the aforementioned covalently functionalized MoS_2 with photoactive species, different photophysical responses have been registered. The MoS_2 entity may act as an energy reflector when carrying a porphyrin, bidirectional electron acceptor when featuring a zinc phthalocyanine, or electron donor and/or energy acceptor when covalently hybridized with carbon dots. Therefore, to unveil MoS_2 electron donor capabilities, a core unsubstituted perylenediimide (PDI) derivative, with proven electron–accepting character, carrying a thiosulfonate moiety, was realized and attached to MoS_2 sulfur-defected edges.[114] The structure of the resulting hybrid is presented in **Figure 6**a. This PDI derivative features a proven electron-accepting character and is selected to explore the electron–donor capabilities of MoS_2. An energy-level diagram (Figure 6b) was designed based

on optical and electrochemical measurements. Briefly, both $^1PDI*$ and $^1MoS_2*$ are capable of promoting electron transfer events upon illumination to yield the $MoS_2^{•+}$–$PDI^{•-}$ CSS. In addition, spectroelectrochemical studies proved the formation of $PDI^{•-}$. Then, fs-TA measurements revealed the formation of $MoS_2^{•+}$–$PDI^{•-}$ CSS by reductive electron transfer to $^1PDI*$ from MoS_2, and the calculated average time constant for the electron transfer was found to be 2.36 ns. With this, now, we have a full picture of the tunable electronic properties of MoS_2 as a result of covalently linking photoactive organic species with precise characteristics.
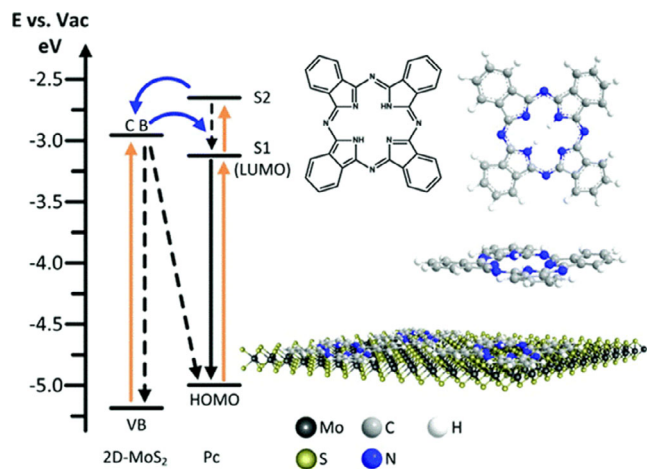
3. Photoinduced Charge Transfer Processes in TMDs Noncovalently Interfacing Photoactive Species

Recent studies related to interaction and electronic communication in supramolecular MoS_2-based donor–acceptor systems are of special interest. In such systems, noncovalent interfacing of porphyrins, phthalocyanines, and other photoactive species on TMDs leads to the realization of ensembles in which the TMDs act either as electron donors or acceptors, depending on the relative energy levels of the organic moieties. This section showcases some of the latest key findings in the study and preparation of supramolecular electron or energy donor–acceptor supramolecular ensembles consisting of TMDs and photoactive molecules.

Liquid-exfoliated MoS_2 nanosheets were used to immobilize via multiple van der Waals forces a free base phthalocyanine (Pc). The so-formed nanoensembles and their optical properties were studied in detail.[115] Photoluminescence and photoelectron spectroscopy in air revealed that the adjusted MoS_2 CB through modification of the lateral size is located between the S_1 and S_2 energy states of the phthalocyanine dye. Therefore, bidirectional photoinduced electron transfer processes were found, with excitation of the functionalized nanosheet's semiconductor transition resulting in electron transfer to the phthalocyanine's LUMO and excitation of the chromophore's S_2 state leading to electron injection into the MoS_2 CB. In other words, phthalocyanine was found to act as either an electron donor or acceptor, depending on the excited transition. However, charge transfer from the dye's S_1 state was not favorable, and consequently, intense luminescence was observed. **Figure 7** shows the energy diagram of the MoS_2/Pc nanoensemble. This is in contrast to the corresponding hybrid material having covalently anchored the ZnPc moiety onto MoS_2, where slow charge separation and recombination were identified.[111] This difference observed is due to the nature of the hybrids examined, film versus solution, and due to the covalent bonding between the donor and acceptor entities.

Continuing with the physisorption of zinc phthalocyanine (ZnPc) onto exfoliated MoS_2, a van der Waals heterostructure was formed and used as a model system to examine charge transfer phenomena at the interface.[116] Photoluminescence measurements and time-resolved two-photon photoemission spectroscopy were used to measure the interfacial charge transfer dynamics. A pump pulse, with a photon energy centered at 1.77 eV chosen to match the S_1 energy of ZnPc, was used to excite the sample. It was found that the optically excited

Figure 6. a) Schematic representation of MoS_2–PDI and b) energy-level diagram depicting reductive electron transfer of $^1PDI*$ and oxidative electron transfer from $^1MoS_2*$ in MoS_2–PDI (thick arrows: most likely process; dotted arrow: less likely process, ET: electron transfer; BET: back electron transfer; T: triplet emission; ISC: intersystem crossing). Reproduced with permission.[114] Copyright 2021, John Wiley and Sons.

Figure 7. Energy-level diagram of MoS$_2$/Pc nanoensemble. Excitation is indicated in orange, radiative recombination processes are indicated in black, and charge transfer in blue. Dashed lines indicate nonradiative processes. Reproduced with permission.[115] Copyright 2019, Royal Society of Chemistry.
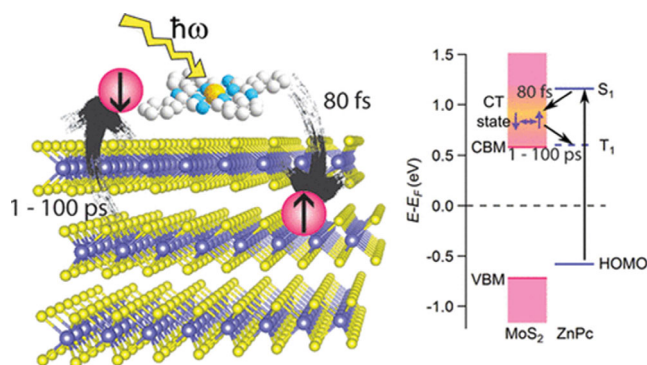

Figure 8. Energy-level diagram of MoS$_2$/ZnPc heterostructure. Reproduced with permission.[116] Copyright 2017, American Chemical Society.

singlet exciton in ZnPc transfers its electron to MoS$_2$ at 80 fs after photoexcitation to form a charge transfer exciton. Nevertheless, back electron transfer occurs in the 1–100 ps timescale, which results in the formation of a triplet exciton in the ZnPc layer (**Figure 8**). This relatively fast singlet–triplet transition is feasible because of the large singlet–triplet splitting in organic materials and the strong spin–orbit coupling in TMD crystals. The back electron-transfer would reduce the yield of free carrier generation at the heterojunction if it was not avoided. In contrast, the spin-selective back electron transfer could be used to manipulate electron spin in hybrid electronic devices.

In parallel, MoS$_2$, MoSe$_2$, and WSe$_2$ were noncovalently functionalized with nickel– or magnesium–phthalocyanines, namely, NiPc or MgPc, as photoexcited electron acceptors, for adjusting the emission and photoresponse of TMDs.[117] Photoexcited electrons were transferred to the metallophthalocyanines (MPcs). Hence, the radiative recombination decreases and leads to emission quenching across the entire TMD flakes. Also, the photo-conductivity of TMDs was increased over twofold as verified by photoconductive atomic force microscopy. Very recently, several MPcs were deposited onto the mechanically exfoliated mono-layer MoS$_2$, and the quenching of the low-temperature (10 K) defect photoluminescence in MoS$_2$ was investigated.[118] The emission quenching was found to crucially depend on the nature of the metal, with the quenching efficiency decreasing in the order CoPc > CuPc > ZnPc, and almost no quenching was observed by the reference metal-free H$_2$Pc. In addition, time-correlated single-photon-counting measurements corroborate this finding, indicating a decrease in the emission lifetime after MPcs adsorption (**Figure 9**). In another investigation, the inter-face properties between MoS$_2$ and differently fluorinated iron Pcs (FePcF$_x$, $x = 0, 4, 16$) were studied using XPS, ultraviolet photoelectron spectroscopy (UPS), angle-resolved photoelectron spectroscopy, and X-Ray absorption spectroscopy.[119] A distinct electron transfer from a molecule to a substrate was observed for FePc and FePcF$_4$. A charge transfer from the chromophores to the MoS$_2$ substrate was detected for the molecules with the lowest ionization potential (FePc and FePcF$_4$), whereas the FePcF$_{16}$–MoS$_2$ interface was relatively inert.

Following a solvothermal route, tetra-*tert*-butyl zinc(II) phthalocyanine (ZnTTBPc) was combined with MoS$_2$ to afford
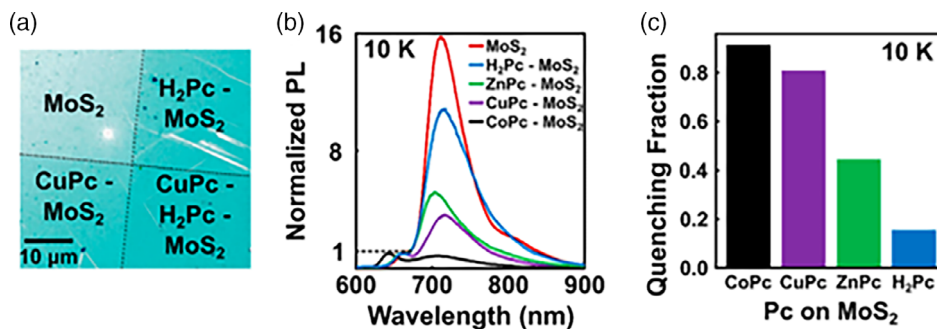
Figure 9. a) Optical microscopy images of representative MPc films on monolayer CVD MoS$_2$. MoS$_2$ emission spectra were collected near the edges of the MPc film to ensure that the observed quenching was not due to inhomogeneity in the CVD growth and b) low-temperature photoluminescence spectra of representative CVD MoS$_2$ and MoS$_2$ with 1 nm films of H$_2$Pc, ZnPc, CuPc, and CoPc. The spectra are normalized to the intensities of their respective MoS$_2$ A-exciton peaks. c) A comparison of the MoS$_2$ defect PL quenching fraction for each MPc. Reproduced with permission.[119] Copyright 2021, American Chemical Society.

ADVANCED
SCIENCE NEWS

www.advancedsciencenews.com

ADVANCED
ENERGY & SUSTAINABILITY
RESEARCH
Open Access

www.advenergysustres.com

MoS_2/ZnTTBPc, with abundant surface photoactive sites. The MoS_2/ZnTTBPc composite showed photocatalytic activity under simulated solar light irradiation for the degradation of 4-nitrophenol. Without going deeper into mechanistic details, a high-energy-transfer efficiency was identified, involving the transfer of photogenerated electrons from the CB of ZnTTBPc to the CB of MoS_2, leaving holes at the VB of ZnTTBPc. Those photogenerated holes at ZnTTBPc are simultaneously quenched and transferred at the VB of MoS_2, sustaining the whole process (**Figure 10**). The aforementioned procedure reduces the recombination of electrons and holes within the composite material and subsequently offers a positive synergetic effect between ZnTTBPc and single-layered MoS_2 nanosheets for the degradation of 4-nitrophenol.[120]

Lately, visible light-absorbing PDIs were physisorbed and integrated onto WS_2 forming supramolecular electron donor–acceptor ensembles (**Figure 11**). In more detail, noncovalent liquid-phase functionalization of 2H-WS_2 allows to bind via σ (WS_2)–π–stacking interactions with PDI derivatives.[121] Detailed spectroscopic investigations of WS_2/PDI confirmed the electron-donating feature of WS_2, along with the electron acceptor properties of PDI. In the ground state, a charge transfer band is observed, which is 29 nm redshifted compared with the

absorption of the PDI reference. This suggests strong electron donor/acceptor electronic interactions in the ground state. Next, photoexcitation at 500 nm leads to the formation of the long-lived (162 ns) $WS_2^{\bullet+}$–$PDI^{\bullet-}$ CSS.

Using a different approach, beyond the aforementioned π–S interactions, stable ternary complexes between benzyl imidazole-modified MoS_2 were interfaced with chromophores in the presence of a cucurbit[8]uril host, to yield in a noncovalent fashion the immobilization of donor and acceptor dyes on the surface of MoS_2, that was further examined by electronic absorption and emission spectroscopy.[122] Naphthol derivative and naphthalene monoimide derivative were selected as the donor and acceptor model chromophores to confirm electronic interaction between the acceptor and the donor molecules with MoS_2 through noncovalent anchoring.

Focusing on Coulombic interactions as meaningful means to interface species without covalently conjugate them, modified semiconducting MoS_2, and WS_2 bearing positively charged ammonium units were electrostatically coupled with an anionic porphyrin possessing a carboxylate group to develop donor–acceptor ensembles,[123] as shown in **Figure 12**. Furthermore, intraensemble interactions were examined by electronic absorption spectroscopy and steady-state and time-resolved photoluminescence titration measurements to identify photoinduced charge transfer between the components. Particularly, the intensity of the porphyrin-centered fluorescence, with maxima at 655 and 720 nm, in benzonitrile was found to depend on the concentration of MoS_2 or WS_2 and progressively quenched, specifying the formation of nanoensemble and possible energy or electron transfer from the porphyrin to TMDs, respectively. In addition, the time-resolved photoluminescence studies revealed faster emission lifetimes for the nanoensembles in comparison with the lifetime of the anionic porphyrin. Overall, these results are characteristic of the photoinduced charge transfer processes from porphyrin to 2H-MoS_2 or 2H-WS_2 acting as an electron or energy acceptor.

Following the aforementioned strategy, namely, using attractive electrostatic interactions, the synthesis of novel donor–acceptor supramolecular nanoensembles consisting of poly (3-thiophene sodium acetate) and ammonium-functionalized 2H-MoS_2 and 2H-WS_2 was accomplished, whereas photoelectrochemical cells were fabricated and tested.[124] Upon titration experiments, a progressive quenching of the emission of the polythiophene derivative at 555 nm revealed photoinduced intra-ensemble energy and/or electron transfer processes from the polymer to the CB of the TMDs. Furthermore, photoelectrochemical studies further confirmed the result of photoinduced charge transfer events in thin films, with distinct responses for the MoS_2- and WS_2-based systems. The MoS_2-based nanoensemble exhibited enhanced photoanodic currents offering additional channels for hole transfer to the solution, while the WS_2-based one exhibited increased photocathodic currents, providing supplementary pathways of electron transfer to the solution.
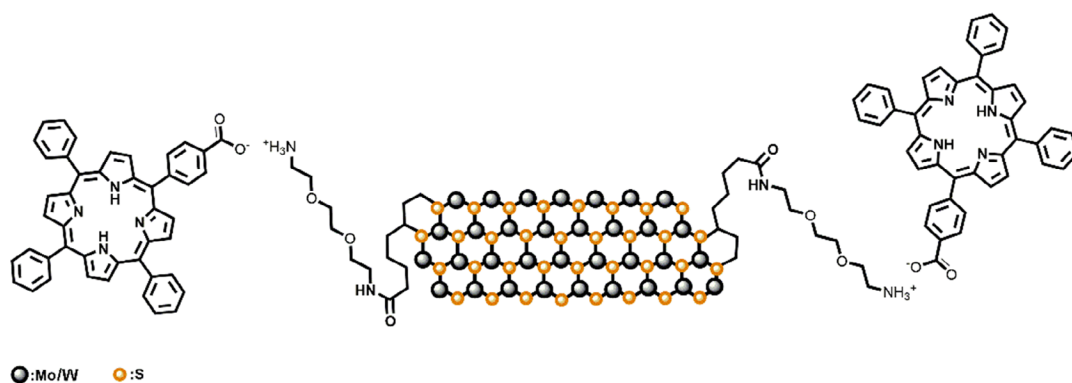
Similarly, ammonium-functionalized semiconducting MoS_2 (f-MoS_2) nanosheets were electrostatically associated with metal nanoclusters (MNCs) based on gold as core and silver as shell, abbreviated as Ag@AuNCs, to form supramolecular hybrids Ag@AuNCs/f-MoS_2.[125] The Ag@AuNCs/f-MoS_2 was applied as a catalyst for wastewater purification from organic pollutant
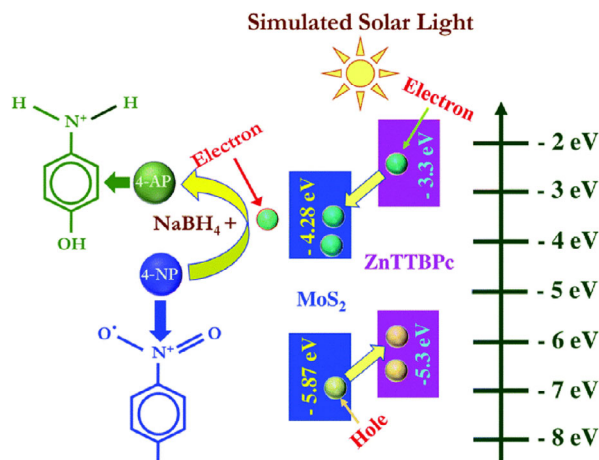
Figure 10. Mechanism of the photocatalytic reduction of 4-nitrophenol using MoS_2/ZnTTBPc under solar light illumination. Reproduced with permission.[120] Copyright 2019, Royal Society of Chemistry.
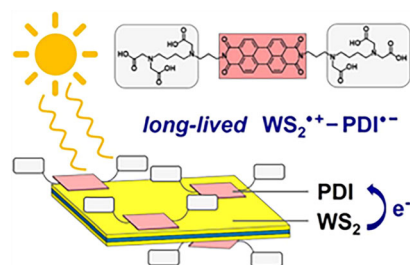
Figure 11. Schematic representation of WS_2/PDI hybrids and photoinduced processes occurring. Reproduced with permission.[121] Copyright 2017, American Chemical Society.

ADVANCED
SCIENCE NEWS

www.advancedsciencenews.com

ADVANCED
ENERGY & SUSTAINABILITY
RESEARCH
Open Access

www.advenergysustres.com

○:Mo/W ○:S

Figure 12. Illustrative structure of the electrostatically interfaced porphyrin to modified MoS_2 and WS_2. Reproduced with permission.[123] Copyright 2018, American Chemical Society.

dyes, for example, for the degradation of rhodamine B. Without going into detail, photoinduced intraensemble charge transfer phenomena were witnessed via photoluminescence (PL) titration assays, and the characteristic emission of Ag@AuNCs at 670 nm was found gradually quenched upon increasing additions of f-MoS_2, showcasing the photocatalytic activity of the hybrid material.

Up to here, the highlighted studies mentioned concern the realization of supramolecularly formed nanoensembles of MoS_2 with photoactive species in solution. However, there have also been few studies performed on thin films. What is more, the presence of a direct bandgap in monolayer TMDs has allowed the construction of prototype optoelectronic devices. Recently, there has been a notable effort to adjust the optical properties of TMDs to improve and optimize the performance of the corresponding devices. In this frame, dye-sensitized MoS_2 photodetectors that utilize a single-layer MoS_2 treated with rhodamine 6G (R6G) organic dye molecules with an optical bandgap of 2.38 eV or 521 nm were developed.[126] The R6G dye molecules deposited onto the MoS_2 layer increased the photocurrent by an order of magnitude due to charge transfer of the photoexcited electrons from the R6G molecules to the MoS_2 layer. In addition, the photodetection response extended to the infrared, thereby distinguishing the device performance from that of a pristine MoS_2 device, in which detection was only possible at wavelengths shorter than the bandgap of MoS_2, that is, <681 nm. The optimized device showed a maximum responsivity of 1.17 AW^{-1}, a photodetectivity of 1.5×10^{-7} Jones, an an external quantum efficiency of 280% at a wavelength of 520 nm, and a photoresponse across a broad spectral range from 980 to 405 nm.

Functionalized MoS_2-based photodetectors with PDIs and tetraphenyl porphyrins using a simple drop-casting method resulted in a dramatic enhancement of the photoresponse and responsivity, three orders of magnitude higher, to visible light.[127] The application of these molecular dyes is an easy and effective route for improving the performance of photodetectors based on 2D materials. In the same line, a metal-free phthalocyanine (H_2Pc) enhances the photoresponse of a monolayer MoS_2 drastically due to the excited-state charge transfer, extending the spectral regions where the TMD is transparent (**Figure 13**).[128] To investigate the excited-state charge transfer at the MoS_2/H_2Pc interface, continuous-wave and time-resolved
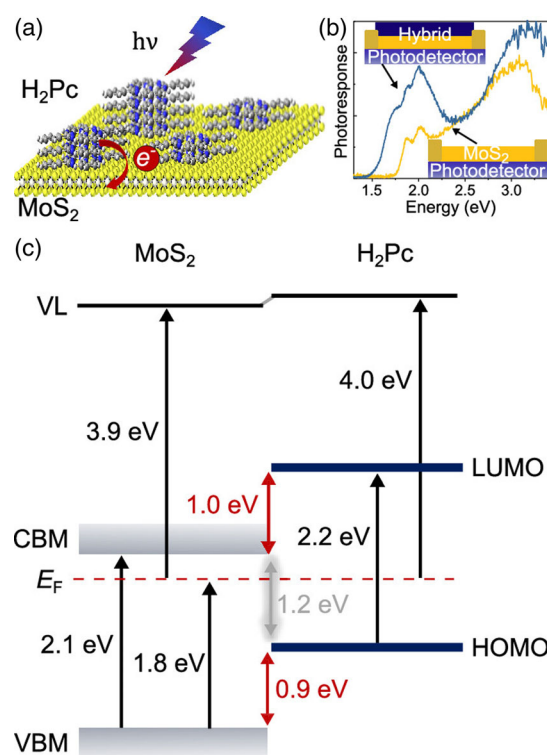
Figure 13. a,b) Schematic representation of a hybrid photodetector, and c) the energy-level diagram of the MoS_2/H_2Pc interface derived from ultraviolet photoemission spectroscopy and inverse photoemission measurements. Reproduced with permission.[128] Copyright 2017, American Chemical Society.

photoluminescence measurements were performed. Time-resolved emission measurements proved highly efficient dissociation of excitons generated in H_2Pc when they are in contact with monolayer MoS_2. A staggered type II energy-level alignment at the interface, facilitating efficient exciton dissociation and excited-state charge transfer with the holes residing in the H_2Pc HOMO and the electrons in the MoS_2 CB, was suggested. In hybrid photodetectors, these transferred charges increase the concentration of carriers in MoS_2 and with that its photoconductivity.

Molecular engineering of large-area MoS$_2$ films with porphyrin dyes was accomplished to enhance their photoelectrochemical properties and to improve the light-harvesting characteristics.[129] Eight different porphyrins were examined, namely, zinc(II)-, iron(III)-, gallium(III)-centered, and metal-free protoporphyrin IX (ZnPP, FePP, GaPP, and H$_2$PP), metal-free and zinc(II)-centered tetra(N-methyl-4-pyridyl)porphines (H$_2$T$_4$, ZnT$_4$), and metal-free and zinc(II)-centered tetraphenylporphyrins (H$_2$TPP, ZnTPP). The porphyrin molecules were physically adsorbed onto large-area MoS$_2$ films that had an average thickness of 2.8 nm. A maximum tenfold increase was observed for MoS$_2$ functionalized with ZnPP compared with pristine MoS$_2$ films, whereas ZnT$_4$-functionalized MoS$_2$ demonstrated small increases in photocurrent. The higher the energy of the HOMO, the greater the photocurrent enhancement produced by the functionalized MoS$_2$ films. The interfacial porphyrins significantly suppress charge recombination pathways and enhance the photocurrent.

Doping method of TMD semiconductors by molecular electron donors or acceptors is one way for optimizing better material's features because of the Fermi-level tuning. The substrate's electrical nature as well as its electronic coupling with the TMDs are also particularly important for charge transfer processes occurring between TMDs and molecular dopants. In a recent study, there are three different charge transfer mechanisms between the molecular electron acceptor 1,3,4,5,7,8-hexafluorotetracyano-naphthoquinodimethane (F$_6$TCNNQ) and a MoS$_2$ monolayer that revealed to be substrate dependent.[130] MoS$_2$ monolayers were grown on sapphire via CVD and transferred onto a highly oriented pyrolytic graphite (HOPG) or Au substrate and then were annealed and F$_6$TCNNQ was deposited in the preparation chamber by sublimation. If there is an insulating substrate, then direct charge transfer between the 2D TMDs valence levels occurs. With a semimetallic substrate, indirect charge transfer from the substrate to the dopant molecule occurs, and at the metallic substrate, the charge transfer occurs from the TMD–metal-hybridized frontier level to the LUMO level of the molecular acceptor (**Figure 14**).

Beyond the immobilization of molecular photoactive species onto TMDs, quantum dots (QDs) or carbon quantum dots (GQDs) interacted with MoS$_2$ nanosheets, exploring photoinduced charge transfer phenomena and enhanced photoresponse in the so-formed nanoensembles. Specifically, MoS$_2$ with oleylamine and dodecanethiol formed stable dispersions of mono- or a few layers in 1,2-dichlorobenzene. The functionalized MoS$_2$ was further utilized for the development of photoactive 0D–2D hybrids with CuInS$_2$ QDs (CIS/MoS$_2$).[131] The QDs were anchored at the surface of MoS$_2$ nanosheets by hydrophobic interactions between the alkyl chain of dodecanethiol molecules present at the surface of both QDs and MoS$_2$. The strong
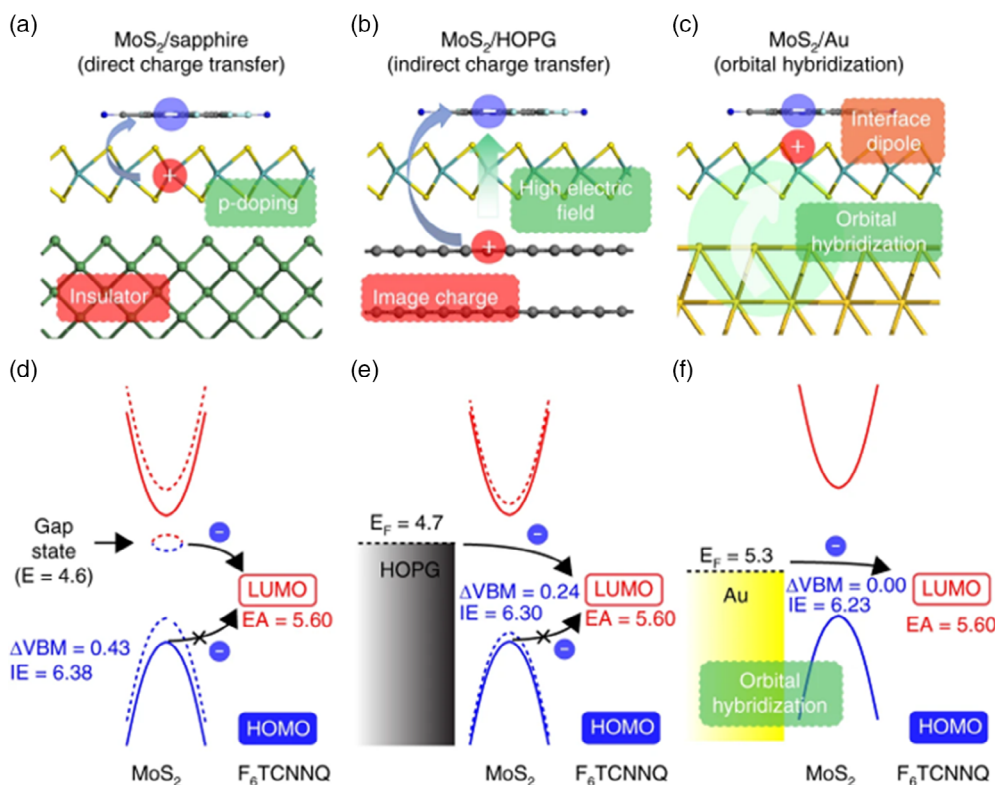
Figure 14. Schematics of the mechanisms of charge transfer between MoS$_2$/substrate and F$_6$TCNNQ. a) Direct charge transfer (MoS$_2$/sapphire, TMDs/insulator), b) indirect charge transfer (MoS$_2$/HOPG, TMDs/weakly interacting conductor), and c) orbital hybridization with charge transfer (MoS$_2$/Au, TMD/strongly interacting conductor). Corresponding energy-level diagrams for d) F$_6$TCNNQ/ML-MoS$_2$/sapphire, e) F$_6$TCNNQ/ML-MoS$_2$/HOPG, and f) F$_6$TCNNQ/ML-MoS$_2$/Au. The solid and dashed lines indicate the levels before and after F$_6$TCNNQ adsorption, respectively. The blue and red lines denote the occupied and unoccupied states, respectively. All the values are given in electron volts (eV). Reproduced with permission.[130] Copyright 2019, Springer Nature.

photoluminescence quenching and decreased emission lifetimes of QDs attached to MoS_2 mark efficient charge transfer from photoexcited QDs to MoS_2. Also, a photoconductive device was fabricated and the photocurrent of the hybrid was dramatically enhanced as compared with QDs or MoS_2-only devices. The great enhancement of photocurrent is attributed to enhance charge separation, charge transfer, and charge carrier transport through a highly conductive network of 2D MoS_2 nanosheets.

Moreover, van der Waals heterostructures using MoS_2 nanosheets-QDs and amine-functionalized GQDs to examine the energy transfer mechanism for tunable PL were constructed.[132] A nonradiative Förster-type energy transfer from GQDs into the MoS_2 layer was confirmed by photoluminescence, time decay analyses, and ab initio calculations. The interaction between the components resulted in quenched emission and a decrease in the time decay of the GQDs.

Finally, QDs were diluted and deposited onto MoS_2 flakes by spin coating via a layer-by-layer process, including the ligand exchange process to form 0D–2D semiconductor hybrids.[133] Layer-dependent electron transfer between core/shell PbS/CdS QDs and layered MoS_2 via energy-bandgap engineering of both
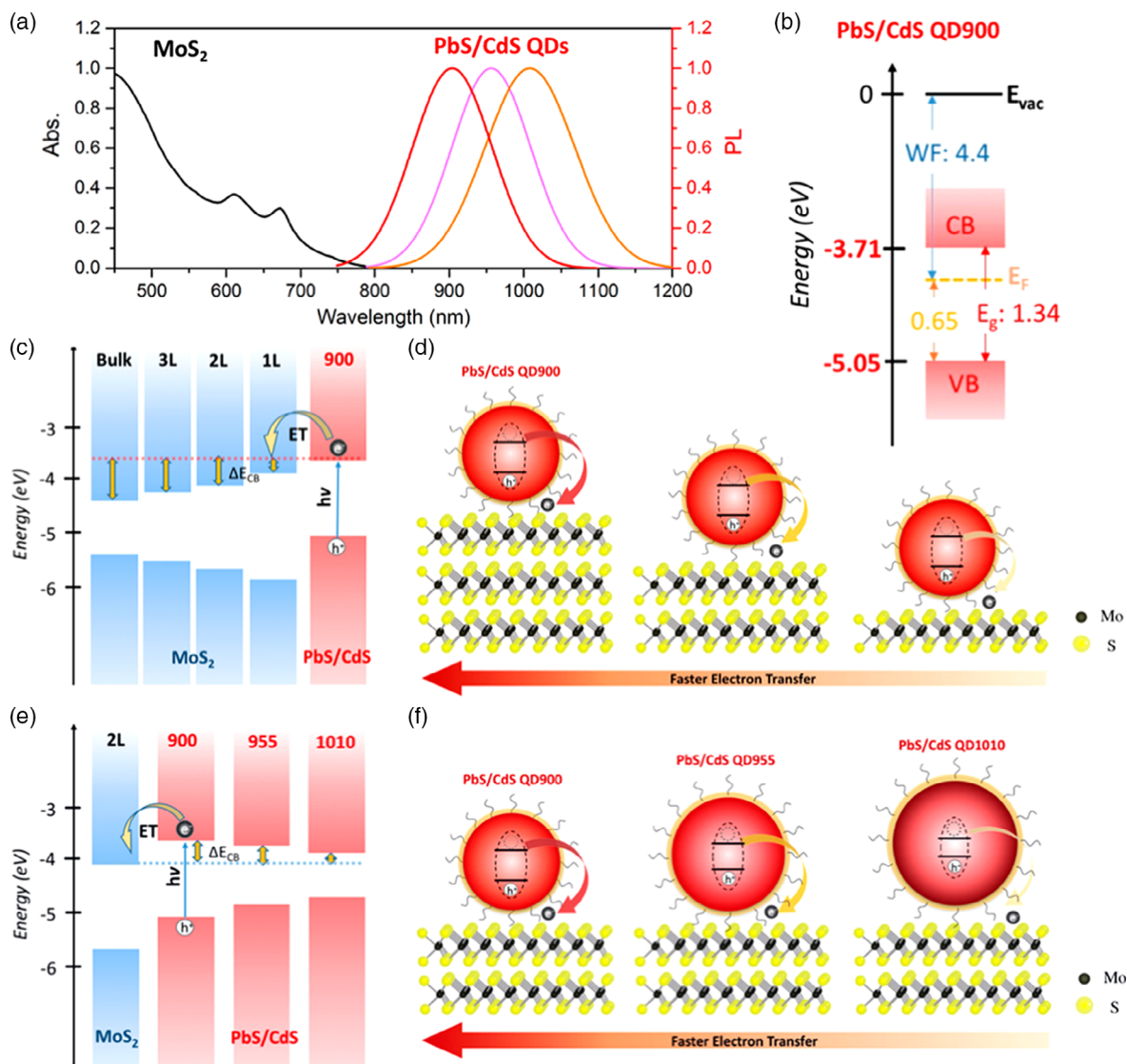
Figure 15. Designed 0D–2D QD/MoS_2 with tunable photoinduced charge transfer. a) Optical absorption and photoluminescence spectra of MoS_2 flakes dispersed in water and of PbS/CdS QDs dissolved in toluene. Emission peaks for PbS/CdS QDs are located at 900 nm (red), 955 nm (purple), and 1010 nm (orange), b) energy levels for the 900 nm emitting PbS/CdS QD with respect to vacuum level as estimated from UPS and absorption spectroscopy (WF, work function; EF, Fermi level; e.g., energy bandgap; CB, conduction band; VB, valence band), c,e) energy band diagrams for monolayer, bilayer, trilayer, and bulk MoS_2 and for PbS/CdS QDs of various sizes/emission colors, and d,f) concept drawing of 0D–2D PbS/CdS QD/MoS_2 hybrids showing bandgap engineering of the acceptor (MoS_2) and donor (QD) in an attempt to tune the charge transfer rate. In (d) PbS/CdS QDs of 900 nm emission are deposited on 1, 2, and 3 layers of MoS_2, and a stronger electron transfer is observed with an increased number of MoS_2 layers. In (f), bilayer MoS_2 is combined with PbS/CdS QDs with PL peaks at 900, 955, and 1010 nm, respectively, with electron transfer becoming stronger with decreased QD size. Reproduced with permission.[133] Copyright 2019, American Chemical Society.

**ADVANCED
SCIENCE NEWS**

www.advancedsciencenews.com

**ADVANCED
ENERGY & SUSTAINABILITY
RESEARCH**
Open Access

www.advenergysustres.com

the donor (QDs) and the acceptor (MoS_2) components was demonstrated (**Figure 15**). Time-resolved confocal emission microscopy, absorption, and photoluminescence spectroscopy were employed. It was found that the charge transfer rate was tuned by changing the size of the QDs or by changing the number of layers of MoS_2, due to the changes in donor–acceptor separation distance and in the bandgap. The charge transfer rate was found higher for QDs of the smallest size and for QDs interacted with a five-layer MoS_2 or thicker.

4. Conclusion and Perspectives

In summary, TMD-based donor–acceptor hybrid materials synthesized via covalent and noncovalent procedures have unveiled strong photoinduced electronic interactions between the participant components. Complementary steady-state and time-resolved photoluminescence and femtosecond transient absorption spectroscopy assays have revealed that these interactions are ascribed mainly to charge transfer phenomena, while in some cases energy transfer prevailed. The ability of tuning the electronic properties of MoS_2, as a result of covalently interfacing photoactive organic species, is a useful strategy that unlocks their potential and exploitation in optoelectronic and light-harvesting applications. The presence of these photoactive species leads to the efficient formation of CSSs. Markedly, MoS_2 modified in a fashion to covalently bearing photoactive organic species acts either as an electron donor, energy or electron acceptor, or bidirectional electron acceptor, depending mainly on the nature and energy levels of the photoactive entity. Although, in covalently modified TMDs, the organic species interfaced are robust and stable, challenging synthetic procedures are needed for the preparation, while the functionalization degree is relatively low. Conversely, noncovalent immobilization of photosensitizers onto TMDs offers notable advantages with respect to covalent approaches, in terms of easiness, versatility, and straightforward preparation. Furthermore, the physisorption of organic photoactive species onto TMDs preserves the excellent optoelectronic properties of TMDs by keeping the crystal structure intact.

Owing to the atomic-scale thickness of TMDs, the direct bandgap of semiconducting TMDs and the possibility of tuning the bandgap upon functionalization hold promise for their utility in a broad range of energy conversion schemes. Currently, the major hindrance to the widespread use of TMD-based materials in nanoelectronics is the small-scale production of these nanosheets. Moreover, although few reports dealing with TMDs for energy conversion exist, the surface functionalization of TMDs with diverse photoactive species beyond the traditionally used ones, for example, porphyrins and phthalocyanines, and the combination of them have yet to be explored. In addition, systematically managing the degree of functionalization in both substrate films and solution-treated prototype devices is of paramount importance. Overall, the use of TMD-based hybrid materials in technologically important applications is anticipated to increase significantly in the near future if those issues and constraints are properly addressed and resolved.

[1] X. Yin, C. S. Tang, Y. Zheng, J. Gao, J. Wu, H. Zhang, M. Chhowalla, W. Chen, A. T. S. Wee, *Chem. Soc. Rev.* **2021**, *50*, 10087.

[2] D. L. Duong, S. J. Yun, Y. H. Lee, *ACS Nano* **2017**, *11*, 11803.

[3] M. Chhowalla, H. S. Shin, G. Eda, L. J. Li, K. P. Loh, H. Zhang, *Nat. Chem.* **2013**, *5*, 263.

[4] Y. C. Lin, D. O. Dumcencon, Y. S. Huang, K. Suenaga, *Nat. Nanotechnol.* **2014**, *9*, 3.

[5] S. J. Sandovsal, D. Yang, R. F. Frindt, J. C. Irwin, *Phys. Rev. B* **1991**, *44*, 3955.

[6] Y. Sun, D. Wang, Z. Shuai, *J. Phys. Chem. C* **2016**, *120*, 21866.

[7] H. R. Gutiérrez, N. Perea-López, A. L. Elías, A. Berkdemir, B. Wang, R. Lv, F. López-Urías, V. H. Crespi, H. Terrones, M. Terrones, *Nano Lett.* **2013**, *13*, 3447.

[8] X. Zhang, Z. Shao, X. Zhang, Y. He, J. Jie, *Adv. Mater.* **2016**, *28*, 10409.

[9] G. Eda, T. Fujita, H. Yamaguchi, D. Voiry, M. Chen, M. Chhowalla, *ACS Nano* **2012**, *6*, 7311.

[10] W. Hu, J. Yang, *J. Mater. Chem. C* **2017**, *5*, 12289.

[11] W. Xia, L. Dia, P. Yu, X. Tong, W. Song, G. Zhang, Z. Wang, *Nanoscale* **2017**, *9*, 4324.

[12] K. Dolui, I. Rungger, C. D. Pemmaraju, S. Sanvito, *Phys. Rev. B* **2013**, *88*, 075420.

[13] C. R. Ryder, J. D. Wood, S. A. Wells, M. C. Hersam, *ACS Nano* **2016**, *10*, 3900.

[14] S. Bertolazzi, M. Gobbi, Y. Zhao, C. Backes, P. Samori, *Chem. Soc. Rev.* **2018**, *47*, 6845.

[15] C. Tan, H. Zhang, *Chem. Soc. Rev.* **2015**, *44*, 2713.

[16] G. Bottari, M. Á. Herranz, L. Wibmer, M. Volland, L. R. Pérez, D. M. Guldi, A. Hirsch, N. Martín, F. D'Souza, T. Torres, *Chem. Soc. Rev.* **2017**, *46*, 4464.

[17] V. Strauss, A. Roth, M. Sekita, D. M. Guldi, *Chem* **2016**, *1*, 531.

[18] A. Stergiou, R. C. Vitoria, M. N. Psarrou, S. P. Economopoulos, N. Tagmatarchis, *Prog. Mater. Sci.* **2020**, *114*, 100683.

[19] A. Stergiou, G. Pagona, N. Tagmatarchis, *Beilstein J. Nanotechnol.* **2014**, *5*, 1580.

[20] A. Agresti, S. Pescetelli, A. L. Palma, B. Martín-García, L. Najafi, S. Bellani, I. Moreels, M. Prato, F. Bonaccorso, A. D. Carlo, *ACS Energy Lett.* **2019**, *4*, 1862.

[21] H. Li, J. Wu, Z. Yin, H. Zhang, *Acc. Chem. Res.* **2014**, *47*, 1067.

[22] P. Sriram, A. Manikandan, F.-C. Chuang, Y.-L. Chueh, *Small* **2020**, *16*, 1904271.

[23] C. F. Zhu, Z. Y. Zeng, H. Li, F. Li, C. H. Fan, H. Zhang, *J. Am. Chem. Soc.* **2013**, *135*, 5998.

[24] N. Rohaizad, C. C. Mayorga-Martinez, Z. S. Orcid, M. Pumera, *ACS Appl. Mater. Interfaces* **2017**, *9*, 40697.

[25] S. Dalgleish, L. Reissig, Y. Shuku, G. Ligorio, K. Awaga, E. J. W. L. Kratochvil, *Sci. Rep.* **2019**, *9*, 16682.

[26] A. Kagkoura, R. Arenal, N. Tagmatarchis, *Adv. Funct. Mater.* **2021**, *31*, 2105287.

[27] K. N. Nazif, A. Daus, J. Hong, N. Lee, S. Vaziri, A. Kumar, F. Nitta, M. E. Chen, S. Kananian, R. Islam, K.-H. Kim, J.-H. Park, A. S. Y. Poon, M. L. Brongersma, E. Pop, K. C. Saraswat, *Nat. Commun.* **2021**, *12*, 7034.

[28] C. R. Ryde, J. D. Wood, S. A. Wells, M. C. Hersam, *ACS Nano* **2016**, *10*, 3900.

[29] J. T. Jang, S. Jeong, J. W. Seo, M. C. Kim, E. Sim, Y. Oh, S. Nam, B. Park, J. Cheon, *J. Am. Chem. Soc.* **2011**, *133*, 7636.

[30] S. Jeong, D. Yoo, J. T. Jang, M. Kim, J. Cheon, *J. Am. Chem. Soc.* **2012**, *134*, 18233.

[31] J. Xie, J. Zhang, S. Li, F. Grote, X. Zhang, H. Zhang, R. Wang, Y. Lei, B. Pan, Y. Xie, *J. Am. Chem. Soc.* **2013**, *135*, 17881.

[32] J. Kwak, S. Jung, N. Lee, K. Thiyagarajan, J. K. Kim, A. Giri, U. Jeong, *J. Mater. Chem. C* **2018**, *6*, 11303.

[33] Y. Liu, N. Zhang, H. Kang, M. Shang, L. Jiao, J. Chen, *Chem. Eur. J.* **2015**, *21*, 11878.

[34] K. S. Novoselov, D. Jiang, F. Schedin, T. J. Booth, V. V. Khotkevich, S. V. Morozov, A. K. Geim, *Proc. Natl. Acad. Sci.* **2005**, *102*, 10451.

[35] A. O'Neill, U. Khan, J. N. Coleman, *Chem. Mater.* **2012**, *24*, 2414.

[36] P. Joensen, R. F. Frindt, S. R. Morrison, *Mater. Res. Bull.* **1986**, *21*, 457.

[37] D. Voiry, M. Salehi, R. Silva, T. Fujita, M. Chen, T. Asefa, V. B. Shenoy, G. Eda, M. Chhowalla, *Nano Lett.* **2013**, *13*, 6222.

[38] Z. Zeng, Z. Yin, X. Huang, H. Li, Q. He, G. Lu, F. Boey, H. Zhang, *Angew. Chem. Int. Ed.* **2011**, *50*, 11093.

[39] A. L. Friedman, A. T. Hanbicki, F. K. Perkins, G. G. Jernigan, J. C. Culbertson, P. M. Campbell, *Sci. Rep.* **2017**, *7*, 3836.

[40] A. Stergiou, C. Stangel, R. Canton-Vitoria, R. Kitaura, N. Tagmatarchis, *Nanoscale* **2021**, *13*, 8948.

[41] G. Pagona, C. Bittencourt, R. Arenal, N. Tagmatarchis, *Chem. Commun.* **2015**, *51*, 12950.

[42] A. Stergiou, N. Tagmatarchis, *Chem. Eur. J.* **2018**, *24*, 18246.

[43] L. Zhou, B. He, Y. Yang, Y. He, *RSC Adv.* **2014**, *4*, 32570.

[44] D. M. Sim, M. Kim, S. Yim, M.-J. Choi, J. Choi, S. Yoo, Y. S. Jung, *ACS Nano* **2015**, *9*, 12115.

[45] E. P. Nguyen, B. J. Carey, J. Z. Qu, J. van Embden, E. D. Gaspera, A. F. Chrimes, M. J. S. Spencer, S. Zhuiykov, K. Kalantar-zadeh, T. Daeneke, *Adv. Mater.* **2015**, *27*, 6225.

[46] J.-S. Kim, H.-W. Yoo, H. O. Choi, H.-T. Jung, *Nano Lett.* **2014**, *14*, 5941.

[47] Q. Ding, K. J. Czech, Y. Zhao, J. Zhai, R. J. Hammers, J. C. Wright, S. Jin, *ACS Appl. Mater. Interfaces.* **2017**, *9*, 12734.

[48] M. Makarova, Y. Okawa, M. Aono, *J. Phys. Chem. C* **2012**, *116*, 22411.

[49] S.-D. Jiang, G. Tang, Z.-M. Bai, Y.-Y. Wang, Y. Hu, L. Song, *RSC Adv.* **2014**, *4*, 3253.

[50] R. Canton-Vitoria, Y. Sayed-Ahmad-Baraza, M. Pelaez-Fernandez, R. Arenal, C. Bittencourt, C. P. Ewels, N. Tagmatarchis, *NPJ 2D Mater. Appl.* **2017**, *1*, 13.

[51] R. H. Goncalves, R. Fiel, M. R. S. Soares, W. H. Schreiner, C. M. P. Silva, E. R. Leite, *Chem. Eur. J.* **2015**, *21*, 15583.

[52] I. K. Sideri, R. Arenal, N. Tagmatarchis, *ACS Mater. Lett.* **2020**, *2*, 832.

[53] D. Voiry, A. Goswami, R. Kappera, C. D. Silva, D. Kaplan, T. Fujita, M. Chen, T. Asefa, M. Chhowalla, *Nat. Chem.* **2015**, *7*, 45.

[54] S. S. Chou, M. De, J. Kim, S. Byun, C. Dykstra, J. Yu, J. Huang, V. P. Dravid, *J. Am. Chem. Soc.* **2013**, *135*, 4584.

[55] Z. Cheng, B. He, L. Zhou, *J. Mater. Chem. A* **2015**, *3*, 1042.

[56] K. C. Knirsch, N. C. Berner, H. C. Nerl, C. S. Cucinotta, Z. Gholamvand, N. McEvoy, Z. Wang, I. Abramovic, P. Vecera, M. Halik, S. Sanvito, G. S. Duesberg, V. Nicolosi, F. Hauke, A. Hirsch, J. N. Coleman, C. Backes, *ACS Nano* **2015**, *9*, 6018.

[57] C. Backes, N. C. Berner, X. Chen, P. Lafargue, P. La Place, M. Freeley, G. S. Duesberg, J. N. Coleman, A. R. McDonald, *Angew. Chem. Int. Ed.* **2015**, *54*, 2638.

[58] A. Tuxen, J. Kibsgaard, H. Gøbel, E. Lægsgaard, H. Topsøe, J. V. Lauritsen, F. Besenbacher, *ACS Nano* **2010**, *4*, 4677.

[59] T. Wang, R. Zhu, J. Zhuo, Z. Zhu, Y. Shao, M. Li, *Anal. Chem.* **2014**, *86*, 12064.

[60] R. H. Goncalves, R. Fiel, M. R. S. Soares, W. H. Schreiner, C. M. P. Silva, E. R. Leite, *Chem. Eur. J.* **2015**, *21*, 15583.

[61] M. Makarova, Y. Okawa, M. Aono, *J. Phys. Chem. C* **2012**, *116*, 22411.

[62] Z. Yu, Y. Pan, Y. Shen, Z. Wang, Z.-Y. Ong, T. Xu, R. Xin, L. Pan, B. Wang, L. Sun, J. Wang, G. Zhang, Y. W. Zhang, Y. Shi, X. Wang, *Nat. Commun.* **2014**, *5*, 5290.

[63] E. P. Nguyen, B. J. Carey, J. Z. Ou, J. van Embden, E. D. Gaspera, A. F. Chrimes, M. J. S. Spencer, S. Zhuiykov, K. Kalantar-zadeh, T. Daeneke, *Adv. Mater.* **2015**, *27*, 6225.

[64] J.-S. Kim, H.-W. Yoo, H. O. Choi, H.-T. Jung, *Nano Lett.* **2014**, *14*, 5941.

[65] K. Cho, M. Min, T.-Y. Kim, H. Jeong, J. Pak, J.-K. Kim, J. Jang, S. J. Yun, Y. H. Lee, W.-K. Hong, T. Lee, *ACS Nano* **2015**, *9*, 8044.

[66] X. Chen, N. C. Berner, C. Backes, G. S. Duesberg, A. R. McDonald, *Angew. Chem. Int. Ed.* **2016**, *55*, 5803.

[67] X. Chen, N. C. Berner, C. Backes, G. S. Duesberg, A. R. McDonald, *Angew. Chem. Int. Ed.* **2016**, *128*, 5897.

[68] M. V. Hidalgo, E. Giovanelli, C. Navío, E. M. Pérez, *J. Am. Chem. Soc.* **2019**, *141*, 3767.

[69] H. Schmidt, F. Giustiniano, G. Eda, *Chem. Soc. Rev.* **2015**, *44*, 7715.

[70] J. Gao, Y. D. Kim, L. Liang, J. C. Idrobo, P. Chow, J. Tan, B. Li, L. Li, B. G. Sumpter, T.-M. Lu, V. Meunier, J. Hone, N. Koratkar, *Adv. Mater.* **2016**, *28*, 9735.

[71] T. Kawanago, S. Oda, *Appl. Phys. Lett.* **2016**, *108*, 041605.

[72] S. Najmaei, X. L. Zou, D. Q. Er, J. W. Li, Z. H. Jin, W. L. Gao, Q. Zhang, S. Park, L. H. Ge, S. D. Lei, J. Kono, V. B. Shenoy, B. I. Yakobson, A. George, P. M. Ajayan, J. Lou, *Nano Lett.* **2014**, *14*, 1354.

[73] M. Gobbi, S. Bonacchi, J. X. Lian, Y. Liu, X.-Y. Wang, M.-A. Stoeckel, M. A. Squillaci, G. D'Avino, A. Narita, K. Müllen, X. Feng, Y. Olivier, D. Beljonne, P. Samorì, E. Orgiu, *Nat. Commun.* **2017**, *8*, 14767.

[74] C. J. L. de la Rosa, R. Phillipson, J. Teyssandier, J. Adisoejoso, Y. Balaji, C. Huyghebaert, I. Radu, M. Heyns, S. De Feyter, S. De Gendt, *Appl. Phys. Lett.* **2016**, *109*, 253112.

[75] Y. Li, C.-Y. Xu, P. Hu, L. Zhen, *ACS Nano* **2013**, *7*, 7795.

[76] D. Kiriya, M. Tosun, P. D. Zhao, J. S. Kang, A. Javey, *J. Am. Chem. Soc.* **2014**, *136*, 7853.

[77] D.-H. Kang, J. Shim, S. K. Jang, J. Jeon, M. H. Jeon, G. Y. Yeom, W.-S. Jung, Y. H. Jang, S. Lee, J.-H. Park, *ACS Nano* **2015**, *9*, 1099.

[78] A. Tarasov, S. Y. Zhang, M. Y. Tsai, P. M. Campbell, S. Graham, S. Barlow, S. R. Marder, E. M. Vogel, *Adv. Mater.* **2015**, *27*, 1175.

[79] D. M. Sim, M. Kim, S. Yim, M.-J. Choi, J. Choi, S. Yoo, Y. S. Jung, *ACS Nano* **2015**, *9*, 12115.

[80] H. Y. Park, S. R. Dugasani, D. H. Kang, J. Jeon, S. K. Jang, S. Lee, Y. Roh, S. H. Park, J. H. Park, *ACS Nano* **2014**, *8*, 11603.

[81] a) Y. C. Du, H. Liu, A. T. Neal, M. W. Si, P. D. Ye, *IEEE Electron Device Lett.* **2013**, *34*, 1328.

[82] D. Çakır, C. Sevik, F. M. Peeters, *J. Mater. Chem. C* **2014**, *2*, 9842.

[83] S. Presolski, M. Pumera, *Mater. Today* **2016**, *19*, 140.

[84] Q. Tang, D. E. Jiang, *Chem. Mater.* **2015**, *27*, 3743.

[85] P. Vishnoi, A. Sampath, U. V. Waghmare, C. N. R. Rao, *Chem. Eur. J.* **2017**, *23*, 886.

[86] C. J. L. de la Rosa, R. Phillipson, J. Teyssandier, J. Adisoejoso, Y. Balaji, C. Huyghebaert, I. Radu, M. Heyns, S. De Feyter, S. De Gendt, *Appl. Phys. Lett.* **2016**, *109*, 253112.

[87] A. Kumar, K. Banerjee, P. Liljeroth, *Nanotechnology* **2017**, *28*, 082001.

[88] B. R. Carvalho, M. A. Pimenta, *2D Mater.* **2020**, *7*, 042001.

[89] X. Zhang, X.-F. Qiao, W. Shi, J.-B. Wu, D.-S. Jiang, P.-H. Tan, *Chem. Soc. Rev.* **2015**, *44*, 2757.

[90] H. Wang, Z. Lu, D. Kong, J. Sun, T. M. Hymel, Y. Cui, *ACS. Nano* **2014**, *8*, 4940.

[91] S. J. Sandoval, D. Yang, R. F. Frindt, J. C. Irwin, *Phys. Rev. B* **1991**, *44*, 3955.

[92] X. Chen, C. Bartlam, V. Lloret, N. Moses Badlyan, S. Wolff, R. Gillen, T. Stimpel-Lindner, J. Maultzsch, G. S. Duesberg, K. C. Knirsch, A. Hirsch, *Angew. Chem. Int. Ed.* **2021**, *60*, 13484.

[93] a) R. Coehoorn, C. Haas, R. A. De Groot, *Phys. Rev. B* **1987**, *35*, 6203; b) Z. X. Gan, L. Z. Liu, H. Y. Wu, Y. L. Hao, Y. Shan, X. L. Wu, P. K. Chu, *Appl. Phys. Lett.* **2015**, *106*, 233113.

[94] X. Geng, W. Sun, W. Wu, B. Chen, A. A. Hilo, M. Benamara, H. Zhu, F. Watanabe, J. Cui, T.-P. Chen, *Nat. Commun.* **2016**, *7*, 10672.

[95] W. S. Yun, S. W. Han, S. C. Hong, I. G. Kim, J. D. Lee, *Phys. Rev. B* **2012**, *85*, 033305.

[96] A. Splendiani, L. Sun, Y. Zhang, T. Li, J. Kim, C.-Y. Chim, G. Galli, F. Wang, *Nano Lett.* **2010**, *10*, 1271.

[97] X. Li, H. Zhu, *J. Materiomics* **2015**, *1*, 33.

[98] R. Ganatra, Q. Zhang, *ACS Nano* **2014**, *8*, 4074.

[99] A. Splendiani, L. Sun, Y. Zhang, T. Li, J. Kim, C.-Y. Chim, G. Galli, F. Wang, *Nano Lett.* **2010**, *10*, 1271.

[100] H. M. Hill, A. F. Rigosi, K. T. Rim, G. W. Flynn, T. F. Heinz, *Nano Lett.* **2016**, *16*, 4831.

[101] R. Ganatra, Q. Zhang, *ACS Nano* **2014**, *8*, 4074.

[102] K. F. Mak, C. Lee, J. Hone, J. Shan, T. F. Heinz, *Phys. Rev. Lett.* **2010**, *105*, 136805.

[103] C. Cong, J. Shang, Y. Wang, T. Yu, *Adv. Opt. Mater.* **2018**, *6*, 1700767.

[104] X. Chen, A. R. McDonald, *Adv. Mater.* **2016**, *28*, 5738.

[105] D. Voiry, A. Mohite, M. Chhowalla, *Chem. Soc. Rev.* **2015**, *44*, 2702.

[106] S. Manzeli, D. Ovchinnikov, D. Pasquier, O. V. Yazyev, A. Kis, *Nat. Rev. Mater.* **2017**, *2*, 17033.

[107] Q. Fu, J. Han, X. Wang, P. Xu, T. Yao, J. Zhong, W. Zhong, S. Liu, T. Gao, Z. Zhang, L. Xu, B. Song, *Adv. Mater.* **2020**, *33*, 1907818.

[108] B. Zhao, D. Shen, Z. Zhang, P. Lu, M. Hossain, J. Li, B. Li, X. Duan, *Adv. Funct. Mater.* **2021**, *31*, 2105132.

[109] D. B. Sulas-Kern, E. M. Miller, J. L. Blackburn, *Energy Environ. Sci.* **2020**, *13*, 2684.

[110] L. Vallan, R. C. Vitoria, H. B. Gobeze, Y. Jang, R. Arenal, A. M. Benito, W. K. Maser, F. D'Souza, N. Tagmatarchis, *J. Am. Chem. Soc.* **2018**, *140*, 13488.

[111] R. C. Vitoria, H. B. Gobeze, V. M. B. Ferrando, J. Ortiz, Y. Jang, F. F. Lazaro, A. S. Santos, Y. Nakanishi, H. Shinohara, F. D'Souza, N. Tagmatarchis, *Angew. Chem. Int. Ed.* **2019**, *58*, 5712.

[112] W. Li, C. He, Y. Dong, W. Song, Y. Zu, *Dyes Pigm.* **2022**, *198*, 109986.

[113] R. C. Vitoria, T. Scharl, A. Stergiou, A. Cadranel, R. Arenal, D. M. Guldi, N. Tagmatarchis, *Angew. Chem. Int. Ed.* **2020**, *59*, 3976.

[114] I. K. Sideri, Y. Jang, J. Garces-Garces, A. Sastre-Santos, R. C. Vitoria, R. Kitaura, F. F. Lazaro, F. D'Souza, N. Tagmatarchis, *Angew. Chem. Int. Ed.* **2021**, *60*, 9120.

[115] E. P. Nguyen, B. J. Carey, C. J. Harrison, P. Atkin, K. J. Berean, E. D. Gaspera, J. Z. Ou, R. B. Kaner, K. Kalantar-zadeh, T. Daeneke, *Nanoscale* **2016**, *8*, 16276.

[116] T. R. Kafle, B. Kattel, S. D. Lane, T. Wang, H. Zhao, W.-L. Chan, *ACS Nano* **2017**, *11*, 10184.

[117] J. Choi, H. Zhang, J. H. Choi, *ACS Nano* **2016**, *10*, 1671.

[118] S. H. Amsterdam, T. K. Stanev, L. Wang, Q. Zhou, S. Irgen-Gioro, S. Padgaonkar, A. A. Murthy, V. K. Sangwan, V. P. Dravid, E. A. Weiss, P. Darancet, M. K. Y. Chan, M. C. Hersam, N. P. Stern, T. J. Marks, *J. Am. Chem. Soc.* **2021**, *143*, 17153.

[119] K. Greulich, A. Belser, S. Bölke, P. Grüninger, R. Karstens, M. S. Sattele, R. Ovsyannikov, E. Giangrisostomi, T. V. Basova, D. Klyamer, T. Chasse, H. Peisert, *J. Phys. Chem. C* **2020**, *124*, 16990.

[120] S. Ibrahim, T. Palb, S. Ghosh, *New J. Chem.* **2019**, *43*, 10118.

[121] T. Scharl, G. Binder, X. Chen, T. Yokosawa, A. Cadranel, K. C. Knirsch, E. Spiecker, A. Hirsch, D. M. Guldi, *J. Am. Chem. Soc.* **2022**, *144*, 5834.

[122] M. Kaur, N. K. Singh, A. Sarkar, S. J. George, C. N. R. Rao, *ACS Appl. NanoMater.* **2018**, *1*, 5101.

[123] R. Canton-Vitoria, C. Stangel, N. Tagmatarchis, *ACS Appl. Mater. Interfaces* **2018**, *10*, 23476.

[124] R. Canton-Vitoria, E. Istif, J. H. Ferrer, E. Urriolabeitía, A. M. Benito, W. K. Maser, N. Tagmatarchis, *ACS Appl. Mater. Interfaces* **2019**, *11*, 5947.

[125] M. A. Koklioti, I. S. Orozcob, M. Quintanab, N. Tagmatarchis, *Mater. Res. Bull.* **2019**, *114*, 112.

[126] S. H. Yu, Y. Lee, S. K. Jang, J. Kang, J. Jeon, C. Lee, J. Y. Lee, H. Kim, E. Hwang, S. Lee, J. H. Cho, *ACS Nano* **2014**, *8*, 8285.

[127] J. Aday, A. J. Molina-Mendoza, L. Vaquero-Garzon, S. Leret, L. De Juan Fernandez, E. M. Perez, A. Castellanos-Gomez, *Chem. Commun.* **2016**, *52*, 14365.

[128] N. Mutz, S. Park, T. Schultz, S. Sadofev, S. Dalgleish, L. Reissig, N. Koch, E. J. W. List-Kratochvil, S. Blumstengel, *J. Phys. Chem. C* **2020**, *124*, 2837.

[129] H. Zhang, J. Choi, A. Ramani, D. Voiry, S. N. Natoli, M. Chhowalla, D. R. McMillin, J. H. Choi, *Chem. Phys. Chem.* **2016**, *17*, 2854.

[130] S. Park, T. Schultz, X. Xu, B. Wegner, A. Aljarb, A. Han, L.-J. Li, V. C. Tung, P. Amsalem, N. Koch, *Commun. Phys.* **2019**, *2*, 109.

[131] R. Ahmad, R. Srivastava, S. Yadav, D. Singh, G. Gupta, S. Chand, S. Sapra, *J. Phys. Chem. Lett.* **2017**, *8*, 1729.

[132] R. Roy, R. Thapa, S. Biswas, S. Saha, U. K. Ghorai, D. Sen, E. M. Kumar, G. S. Kumar, N. Mazumder, D. Roya, K. K. Chattopadhyay, *Nanoscale* **2018**, *10*, 16822.

[133] J.-S. Chen, M. Li, Q. Wu, E. Fron, X. Tong, M. Cotlet, *ACS Nano* **2019**, *13*, 8461.

Christina Stangel is a postdoctoral researcher in Theoretical and Physical Chemistry Institute at the National Hellenic Research Foundation, in Athens (Greece). Her research interests mainly focus on the chemistry of tetraazamacrocycles and surface functionalization of low-dimensional carbon-based materials toward energy conversion applications.

ADVANCED
SCIENCE NEWS

www.advancedsciencenews.com

ADVANCED
ENERGY & SUSTAINABILITY
RESEARCH
Open Access

www.advenergysustres.com

Eleni Nikoli is a Ph.D. candidate in Theoretical and Physical Chemistry Institute at the National Hellenic Research Foundation, in Athens (Greece), under the supervision of Dr. Nikos Tagmatarchis. She received her B.Sc. from the University of Patras in 2017 and M.Sc. from the National Technical University of Athens in 2019. Her research interests mainly focus on the chemical functionalization of 2D nanostructured materials and the investigation of their charge transfer phenomena.

Nikos Tagmatarchis is the Director of the Theoretical and Physical Institute, National Hellenic Research Foundation, in Athens, Greece. His research interests focus on the chemistry of 2D nanomaterials and carbon nanostructures, particularly in the context of energy conversion and storage applications. His accomplishments in the area are reflected in a plethora of publications, with multiple citations and numerous invitations at conferences. He has been the recipient of the European Young Investigator Award (2004), Visiting Professor at the Chinese Academy of Sciences (2011–2012), Invited Fellow by the Japan Society for the Promotion of Science (2013–2014 and 2018), and Chemistry Europe Fellow Class 2018/2019.